The Transition of the Hurricane Frederic Boundary-Layer Wind Field from the Open Gulf of Mexico to Landfall

MARK D. POWELL

National Oceanic and Atmospheric Administration, National Hurricane Research Laboratory, Coral Gables, FL 33146

ABSTRACT

Numerous aircraft, ship, buoy and land station data were composited with respect to the center of Hurricane Frederic for two time periods: a 24 h period corresponding to the storm's position in the open Gulf of Mexico on 12 September 1979, and an 8 h period corresponding to the landfall of Frederic near 0400 GMT on 13 September. Comparison of wind analyses for the two periods indicated a rotation of maximum inflow angles from the southeast to northeast quadrants and a strong frictional decrease of wind speed over land. These and other features of the landfall analysis were compared with a model landfall study by Moss and Jones (1978). The landfall composite wind field was compared with the Fujita damage vector analysis to determine the damage time interval and mean wind speed range. Damage vector directions were found to be well correlated with the surface streamlines, with the most severe damage being associated with Frederic's northern eyewall.

Ten-meter-level wind speed data over water (V_0) and at coastal stations (V_L) were used to formulate approximate relationships of the low-level (500–1500 m) aircraft wind (V_a) to the mean coastal wind and peak gust (V_{LG}) in the same position relative to the storm center. It was found that $V_0 = 0.7V_a$, $V_L = 0.8V_0$, $V_{LG} = 0.8V_a$ and $V_L = 0.56V_a$. These relationships should aid forecasters in their assessments of low-level aircraft reconnaissance wind data for use in issuing warnings.

The vertical shear of the horizontal wind determined from radiosonde data for two inland stations was compared with shear determined from surface and aircraft data over water. The overland shear was greater than the overwater shear, by a factor of 2, in the same relative part of the storm. The "thermal wind" shear computed in the vicinity of the center was negligible, although the 10 m level air temperature analysis over land indicated a cold core that was probably caused by adiabatic cooling.

1. Introduction

Tropical cyclones undergo a major transition when approaching land from the open water. Land induces frictional and thermal effects that change the turbulent wind structure responsible for much of the damage. To forecast the behavior of a tropical cyclone when it is approaching land and to effect proper warnings, we must understand the physical changes in the storm during the landfall process. The Hurricane Strike program at the National Hurricane Research Laboratory (NHRL) is directed at investigation of these changes and the landfall process.

Hurricane Frederic struck the Alabama–Mississippi Gulf Coast in September 1979 causing widespread wind and storm surge damage. Frederic's track through the Gulf of Mexico, and landfall in the moderately populated Pascagoula–Mobile area, make it one of the best-documented hurricanes in history. Frederic was monitored for 3 days, before, during and after landfall by seven National Oceanic and Atmospheric (NOAA) Research Facility Center (RFC) scientific reconnaissance flights, numerous ship and buoy platforms in the open Gulf of Mexico, and many land stations. From these observations, we created a data base from which the surface wind field of the storm could be documented during the transition from the open Gulf of Mexico to landfall.

The object of this paper is to show, through analysis of the low-level wind field, the changes in boundary-layer structure and some of the physical mechanisms responsible for these changes during the transition. Previous hurricane wind field studies are discussed, the procedure for compositing Frederic data with respect to the storm center for the two time periods is described, and analyses of the surface wind fields are used to describe physical changes in the hurricane's structure. Relationships of the aircraft wind to the coastal mean wind and peak gust are presented for possible use in forecast guidance and the surface wind field is compared with the damage field.

2. Background

One of the first observational studies of the surface wind field in hurricanes was made by Myers (1954a). He analyzed data collected from observing stations in and around Lake Okeechobee for 1949 and 1950 hurricanes and also studied characteristics of numerous storms from 1900 to 1950. His study was followed

by 1000 ft aircraft data analyses from Pacific storms by Hughes (1952), a three-dimensional wind field composite by Miller (1958), composites of ship data from six hurricanes by Krueger (1959), and composite wind field analyses of 14 hurricanes from 1821 to 1957 by Graham and Hudson (1960).

Several studies were made of the effect of friction on the storm at landfall, and how this effect differed over land and water. These included further studies on the Lake Okeechobee data set by Johnson (1954) and Myers (1954b), and studies on several hurricanes by Hubert (1955, 1959) and Malkin (1959). Miller's (1963, 1964) composite study of Hurricane Donna in 1960 was the first to indicate that the main reason for weakening of a hurricane after landfall was the loss of its latent heat source. In another composite study, Bradbury (1971) studied changes in the surface pressure field and radar echo motion field for two 9 h periods before and after the landfall of Hurricane Camille in 1969.

To depict the surface wind field, models by Myers and Malkin (1961) and Chow (1971) were constructed from the observed characteristics of storms and according to the earlier studies. The models differed in the parameterization of friction and the resulting wind fields differed in the position of asymmetries. Recently, more sophisticated models by Moss and Jones (1978) and Tuleya and Kurihara (1978) have been employed to study the effects of landfall on a storm. The Moss and Jones study indicated a rotation of the region of maximum surface winds from the right side to the landward front side of the storm, with an increase in the wind speed as the storm approached land. Verification of such a feature in nature could have far-reaching implications in issuing warning and intensity forecasts for landfall. Some suggestion of this effect is evident in a study by Smith (1975), who used synoptic observations and Air Force reconnaissance reports to study the intensification of Hurricane Celia in 1970. His results indicate a surface wind speed maximum on the landward left front side, which compared well with results found by Fujita (1980).

Other studies have dealt with wind engineering and damages produced by extreme hurricane winds and tornadoes. Fujita (1971) developed a scale, the "*F*" scale, for use in relating observed wind damage in tornadoes and hurricanes to wind speed. Although the *F* scale was developed to be applied primarily to tornado damage, Fujita (1980) has also applied it to damage caused by Hurricanes Celia, Camille and Frederic. Novlan and Gray (1974) composited data from many storms in a study of hurricane-spawned tornadoes and their relation to vertical wind shear. Reinhold and Mehta (1981) made careful analyses of several land-based anemometer records in Hurricane Frederic to characterize "design wind" parameters according to observed structural damages.

The quantity of wind observations in Frederic, from several sources, provides a greater coverage of data than has previously been available in earlier investigations, especially over water. These data, with an analysis method capable of isolating land and sea effects, permit the first available observational study of the transition of the mesoscale wind field during landfall.

3. Procedures

In this section a brief review of the history of Frederic is followed by discussion on the time periods chosen for the composites, the advantages of the compositing technique, and the steady-state approximation during the composite time period. Data sources and sampling intervals are discussed and the analysis procedures and techniques are explained.

a. Storm history

Frederic reintensified into a hurricane at 1200 GMT 10 September 1979 over the western end of Cuba and moved north–northwest for the next three days, making landfall just east of the Alabama–Mississippi border at 0400 GMT 13 September. Further information on the life cycle and development of Frederic can be found in Hebert (1980). The track of Frederic, including maximum flight-level sustained wind speeds, and minimum sea-level pressures, is shown in Fig. 1.

b. Composite time periods

The 24 h period from 1600 GMT 11 September until 1600 GMT 12 September was chosen for the first composite period, henceforth designated "overwater." An 8 h period from 0000 GMT 13 September until 0800 GMT 13 September was chosen for the second composite and is designated "landfall."

The overwater composite period was chosen to allow a data coverage that would present a "synoptic" representation of the hurricane in the central Gulf of Mexico with no land influences. Two low-level aircraft flights and a NOAA Data Buoy Office (NDBO) buoy sampled the inner 220 km of the storm, while additional buoys and ships sampled the storm at radial distances > 220 km. The data coverage during the overwater composite is shown in Fig. 2. Some of the data from densely plotted regions were removed from Fig. 2 to clarify the presentation. The data were plotted with respect to land for the storm track position that applies to the middle of the composite time period (0400 GMT, 12 September). All overwater composite analyses apply to 0400 GMT.

The landfall composite period was chosen to allow a data coverage that would be representative of the storm during the passage of the eye from water to land (~0400 GMT, 13 September) and also to apply to a synoptic view of the storm at the time of max-
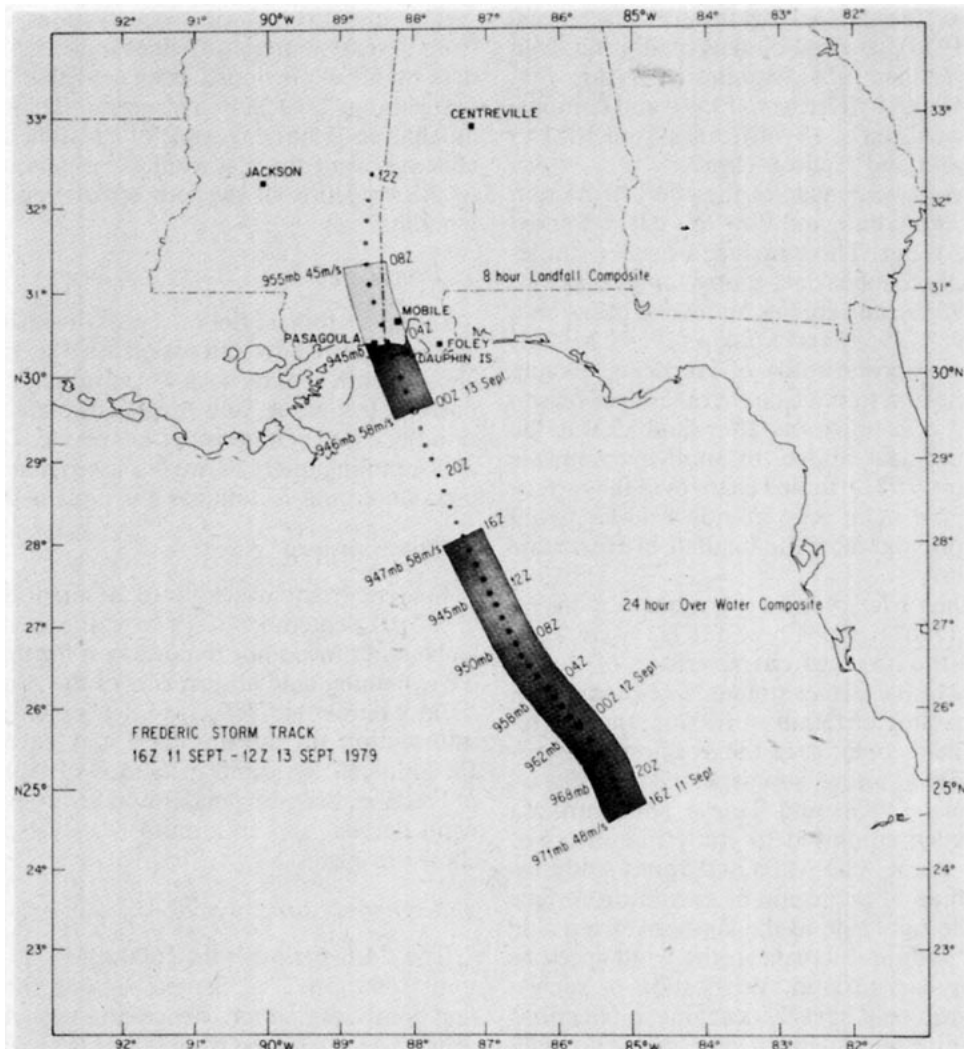
FIG. 1. Storm track and composite time periods for Hurricane Frederic. Hourly positions are noted in "Z" (GMT). Composite time periods are shaded; minimum pressures and maximum sustained wind speeds are included.

imum coastal winds (65 m s^{-1} gust at the Dauphin Island Bridge near 0200 GMT). The landfall composite period includes the final penetrations of the eye by research aircraft before landfall, data during landfall from flights parallel to the coast, and hourly observations from land stations and ships.

An 8 h period was required to provide a data coverage similar to the overwater composite. The data coverage for the landfall composite is presented in Fig. 3 in the manner of Fig. 2. The data were plotted with respect to land for the 0200 GMT storm track position. At this time, maximum winds were experienced at the coast. All landfall composite wind field analyses apply to 0200 GMT.

c. Composite advantages and assumptions

The advantages of the composite technique include:

1) Improvement of data coverage by alleviation of data voids that occur with synoptic analysis.

2) A check on consistency through comparison of adjacent observations at similar radial distances, but at different times.

3) Elimination of small-scale and short-time period data fluctuations, unless such fluctuations persist for several data sources. The analyses are assumed to be comparable to synoptic fields that apply to the storm near the middle of the composite time period.

To achieve the above advantages, two assumptions must be made:

1) The storm is in an approximate steady-state condition. Ideally, a high density grid of synoptic observations would be most desirable for a study of this type. Since this is not possible, the best approximation to the ideal case is a set of observations com-
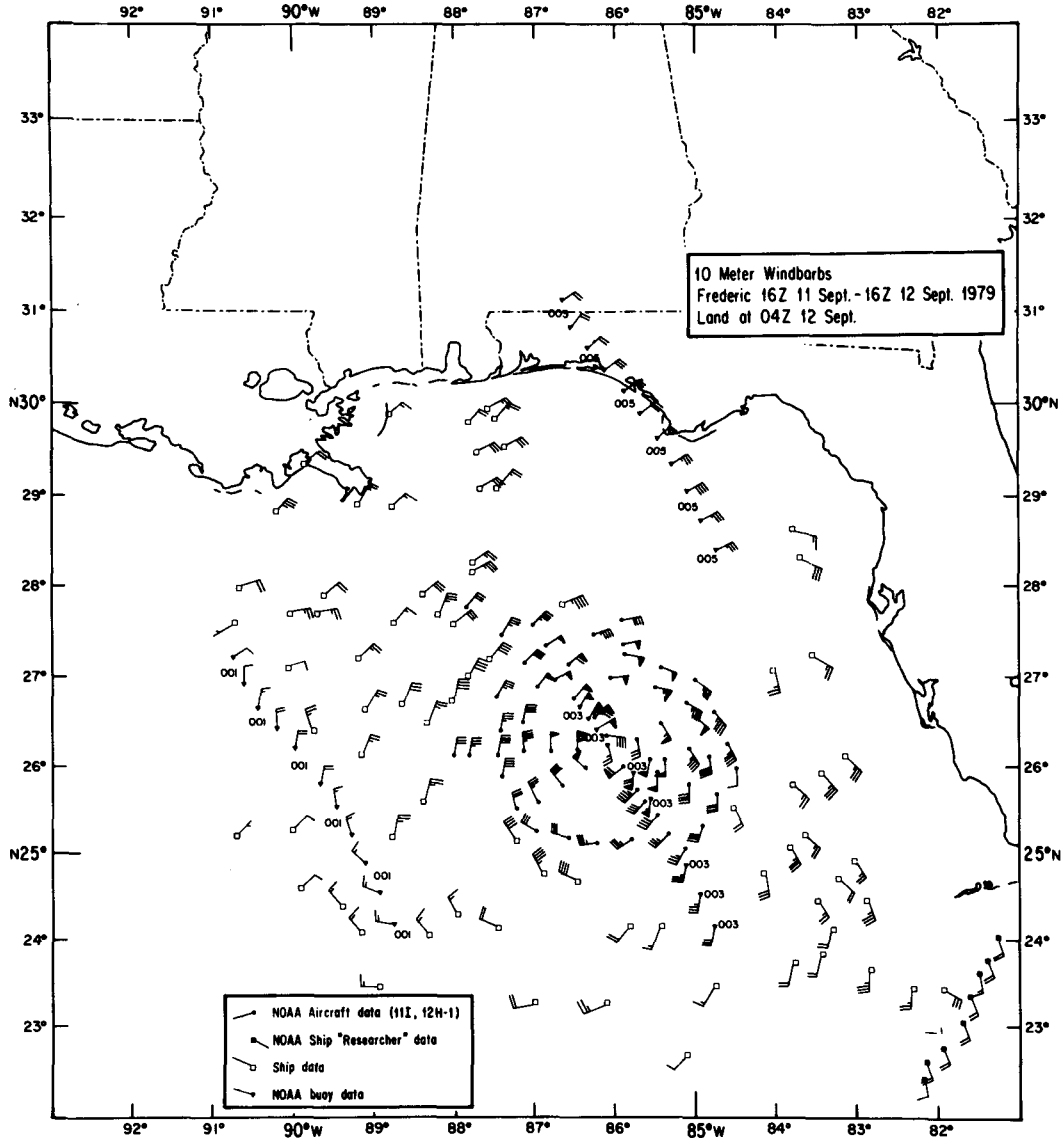
FIG. 2. Data coverage for the overwater composite. Numbers refer to NDBO buoys. Wind barbs at 10 m level correspond to conventional plotting, with speeds in knots.

posited with respect to the storm center over a time period of minimal intensity changes. Changes of storm intensity are related to changes in the minimum sea-level pressure, maximum average wind speed and radius of maximum wind. For a steady state approximation to apply, intensity changes must be minimized. This assumption is discussed in Section 3d.

2) The measurement techniques, sampling times and exposures from the various observational platforms used in the composites are equivalent. This assumption is discussed in Sections 3e and f.

d. The steady-state approximation

The basic assumption for the composite method is that the storm is in an approximate steady state

throughout the composite period. The over-water composite involved a storm motion of 5 m s⁻¹ and a pressure drop from 971 to 945 mb, for an average drop of 1 mb per hour, while the maximum sustained flight-level wind speed increased from 48 to 58 m s⁻¹. The pressure drop rate is approximately the same as that which occurred in Donna during the two over-water 12 h composite periods used by Miller (1963). From 0600, 12 September to ~0400, 13 September, the central pressure varied only betwen 952 to 945 mb. Therefore, the storm was considered to be approximately steady-state from the last half of the over-water composite until landfall. Aircraft data collected during the entire overwater composite time period were compared in order to insure analyses representative of steady-state conditions.
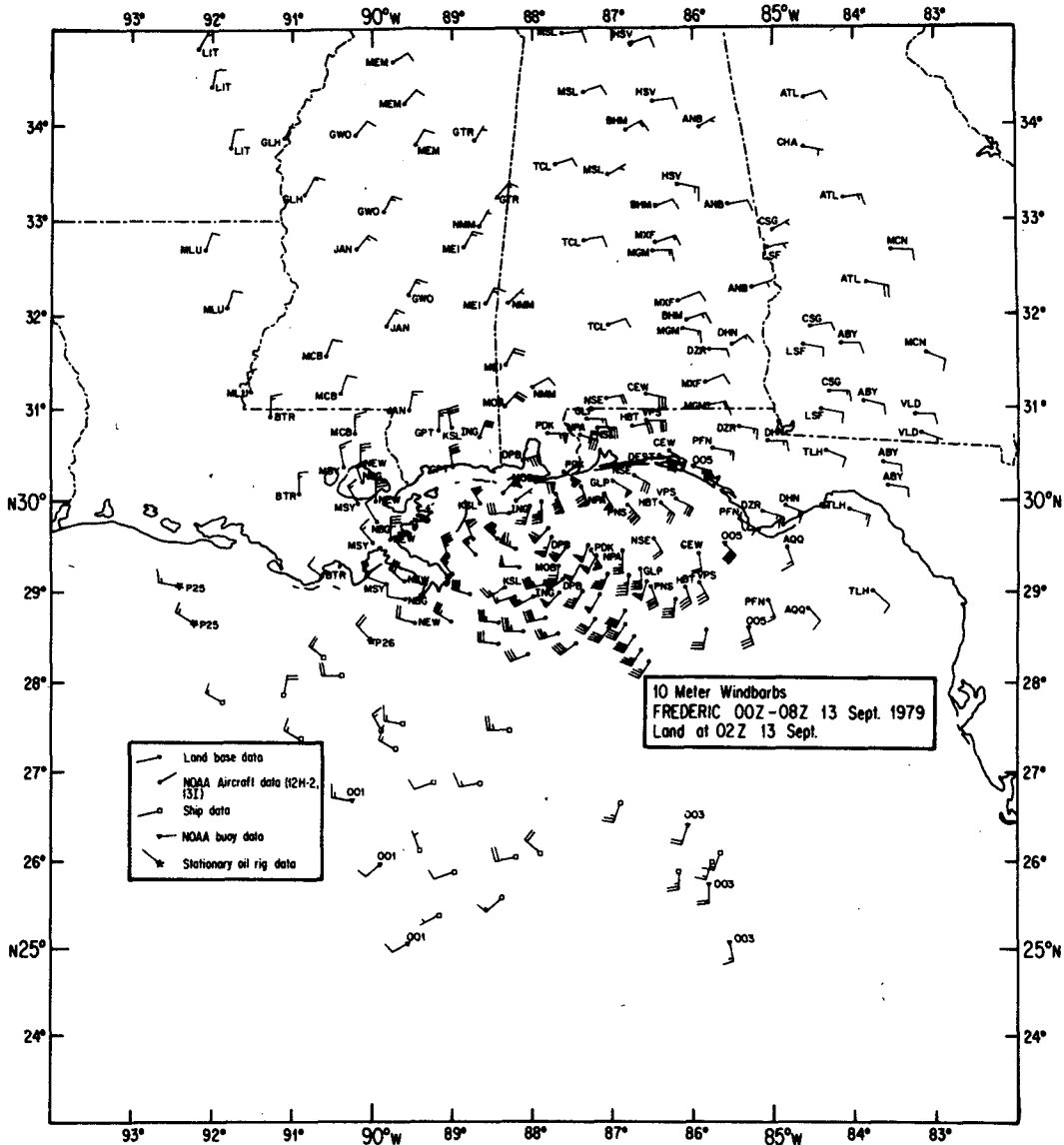
FIG. 3. As in Fig. 2, except for landfall composite.

The wind field during the two NOAA research flights in the overwater period was remarkably constant outside a radial distance of 40 km from the storm center. The radius of maximum winds (R_{max}) and the maximum 30 s average flight-level wind (V_{max}) varied depending upon the quadrant penetrated and time. The mean R_{max} decreased from ~33 to 27 km; the central pressure dropped from 960 to 948 mb and the V_{max} increased from 48 to 58 m s^{-1} from late (2300 GMT) 11 September (designated the 11 I flight) to early (0700 GMT) 12 September (the 12 H1 flight), respectively. These changes are illustrated in Fig. 4, which details profiles of surface pressure and wind speed on the north side of the storm at the 500 m altitude during the 11 September and 12 September flights. Outside 40 km, the radial

surface pressure gradients and the flight-level wind speeds are essentially equal for both flights, while inside 40 km, the surface pressure gradient and wind speeds are stronger for the 12 September flight. Several passes in other quadrants of the storm indicated a similar tendency.

In the overwater isotach analyses that follow, the data within 40 km were analyzed for the winds measured during the 12 September flight, whereas the wind speeds analyzed outside 40 km are representative of both flights. Data coverage was augmented by NOAA buoy 42003 observations which minimized any loss from neglecting the 11 September flight data within 40 km. This method of analysis results in a wind field that is representative of the center time of the composite (0400 GMT 12 September) and min-
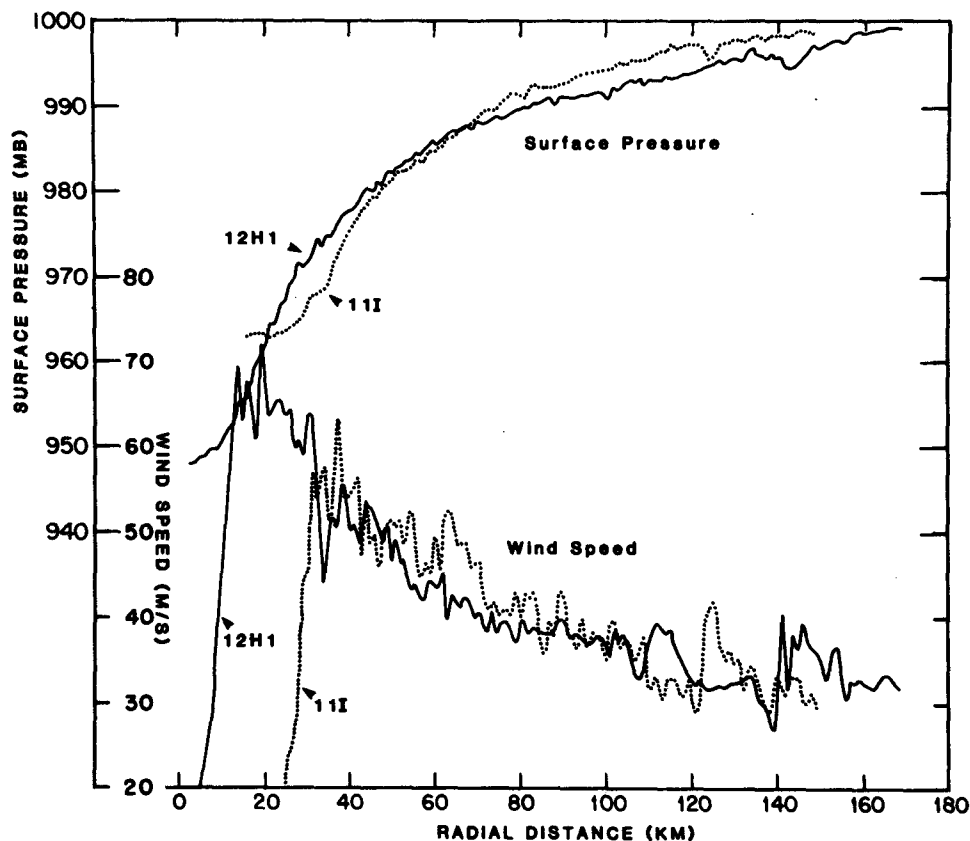
FIG. 4. Radial profiles of windspeed and surface pressure on the north side of Frederic
at the 500 m level for the 11 September (11 I) and 12 September (12 H1) flights.

imizes any possible errors caused by violation of the steady-state approximation in the first half of the over-water composite.

The landfall composite period (0000–0800 GMT 13 September) contains a rise in central pressure from 946 to approximately 955 mb, a storm motion of 6.5 m s⁻¹, and a decrease in maximum average flight-level winds from 58 m s⁻¹ to an estimated 45 m s⁻¹. The minimum sea-level pressure measured over land in the storm was 946 mb at Ingalls Shipyard in Pascagoula, Mississippi, at 0400 GMT 13 September. This compares well with the minimum aircraft-computed sea-level pressure at 0300 GMT. However, from 0400 to 0800 GMT there were no stations close enough to the storm to determine how much filling had occurred. Pressure relationships for filling after landfall, by Myers (1954) and Malkin (1959), estimate a central pressure increase from the landfall pressure of 945 mb to 952 and 955 mb, respectively for the 4 h from 0400 GMT to 0800 GMT 13 September. Most of the pressure change occurred in the second half of the landfall composite time period. Although the composite time period consisted of data taken four hours before and after landfall, the objective of the analyses was to depict the wind field of the storm at its most destructive state during landfall.

Therefore, the analyses were mapped to be applicable to the time at which the maximum winds were measured on the coast at Dauphin Island Bridge (0200 GMT 13 September) while the storm center was still offshore. Nearly all of the land observations within two degrees of latitude of the storm center were taken in the first half of the composite period between 0000 and 0400 GMT, thus minimizing the affect of later pressure rises on the steady state assumption.

e. Data sources and sampling

Surface observations consisted of data from 91 land sources (NOAA, FAA, Coast Guard, private sources), 3 NDBO buoys, 54 ships of opportunity and 4 NOAA research aircraft flights. Over land, data were corrected to a common height of 10 m by power law with a power corresponding to the estimated terrain type (Reinhold and Mehta, 1980). This correction was small, since the mean anemometer height over land stations was 7.5 m.

Over water, the majority of wind data beyond 175 km from the storm center were from ship observations of the sea state (Beaufort wind force) and a few measured ship winds. On ships lacking wind measuring equipment, wind speed was estimated accord-

ing to National Weather Service (NWS) standards from Beaufort force observations. Beyond 175 km of the storm center, ship wind speeds ranged from 10 to 20 m s^{-1} and were assumed to apply to a mean anemometer height of 19.5 m (V. Cardone, personal communication, 1981). These, with aircraft flight-level observations and buoy observations, were adjusted to 10 m by a diagnostic boundary-layer model (a combination of the Powell and Moss-Rosenthal models discussed in Powell, 1980). The various observation platforms comprise several averaging periods ranging from 30 s to 20-30 min. While none of the platforms can be considered entirely equivalent, it is useful to discuss their approximate equivalence in terms of the portion of the storm measured during the observation.

NDBO buoys employed 8.5 min averages, and aircraft data consisted of 30 s averages. The aircraft averages corresponded to a 3 km sampling of the storm at an aircraft speed of 100 m s^{-1}. For the overwater composite, during which the storm moved at a mean speed of 5 m s^{-1}, NDBO buoys sampled a 2.5 km (5 m s^{-1} × 8.4 min) section of the storm. Ship wind measurements consisted of 1 min averages and corresponded to a 0.3 km sampling of the storm. Wind speed estimates from Beaufort force observations are believed to be applicable to a 20-30 min average (D. Ross and V. Cardone, personal communication, 1981). It was inferred by Pierson et al. (1980) that a 20-30 min average is a good estimate of the synoptic scale wind speed. A 20-30 min average corresponds to a 6.0-9.0 km sampling distance of the storm. Beyond 175 km, where wind speeds reached a maximum of 20 m s^{-1}, the majority of observations were Beaufort force estimates. Additional observations were from two NDBO buoys and a few ship anemometers. Although storm sample distances for these platforms vary from 0.3 to 6.0 km, the observations from the different platforms compared well when plotted with respect to the storm center. Within 175 km of the storm center during the over-water composite, only buoy and aircraft measurements were available, and appear to be equivalent based on sampling distances. For the purposes of this study, the over-water observations appear to be approximately equivalent and no corrections were made to the data. Most of the land-based observations involved wind speed determined from an hourly 1 min average, the exception being private or municipal anemometer chart records from which an average was taken that would correspond to 5-10 min. In the landfall composite, 10 stations with wind observations were within 110 km of the center. Anemometer charts were available for six of the 10 stations including the three stations closest to the storm center, Dauphin Island Bridge (DPB), Ingalls Shipyard (ING) and the Mobile National Weather Service Office (MOB).

Durst (1960) statistically derived relationships between wind speeds averaged over various time periods and measured over flat terrain. He determined that in strong winds (20-40 m s^{-1}),

$$V_{10} = 0.86 V_1, \qquad (1)$$

where V_{10} and V_1 are 10 min and 1 min probable maximum wind speed averages, respectively, over an hour. Although anemometer chart-determined wind speeds could be <1 min observations, no systematic differences could be determined from the composited land data. Furthermore, at a storm speed of 6.5 m s^{-1} during the landfall composite, a 5-10 min average corresponds to a storm sampling of ~3 km, which is equivalent to the aircraft observations that make up the bulk of the data over water. Therefore, for both the overwater and landfall composites, the observation platforms appear to be equivalent in terms of sampling the wind field of the hurricane and no corrections were applied to the data.

f. The analysis technique

To properly composite the data with respect to the storm center for both composite analysis periods, polynomial fits were made of the storm latitude and longitude as a function of time. For each station, virtual latitude (V_{LY}) and longitude (V_{LX}) were computed by subtracting the storm position from the station position. The V_{LX} and V_{LY} were then converted to X, Y positions and the station was plotted on a Mercator projection with respect to the storm center. Only stations within the 550 km of the storm center were plotted.

1) OVERWATER ANALYSES

When the over-water composite was produced, buoy wind speeds in the northwest and southeast quadrants were found to compare well with 10 m level model-computed aircraft wind speeds. Comparison of buoy and aircraft flight level wind directions, however, indicated a veering with height of 10-15° in the northwest quadrant and 30-50° in the southeast quadrant.

Similar veering was observed in Hurricane Eloise (1975) by Peter Black (personal communication, 1981, NHRL) from comparisons of surface wind directions deduced from airborne vertical camera photographs of the sea surface (See Fig. 5). The larger directional shear in the rear of the storm is probably caused by stable conditions over the cold sea surface "wake" of the storm. The cool wake is a common feature in hurricanes and is caused by upwelling (Black, 1972).

Unfortunately, no vertical camera data were available for Hurricane Frederic, and the boundary-layer model used to calculate 10 m level winds from aircraft data is not capable of computing surface wind directions. Therefore, the overwater streamline analysis that follows (Fig. 6) weights the buoy and ship directional data more heavily than the aircraft data.
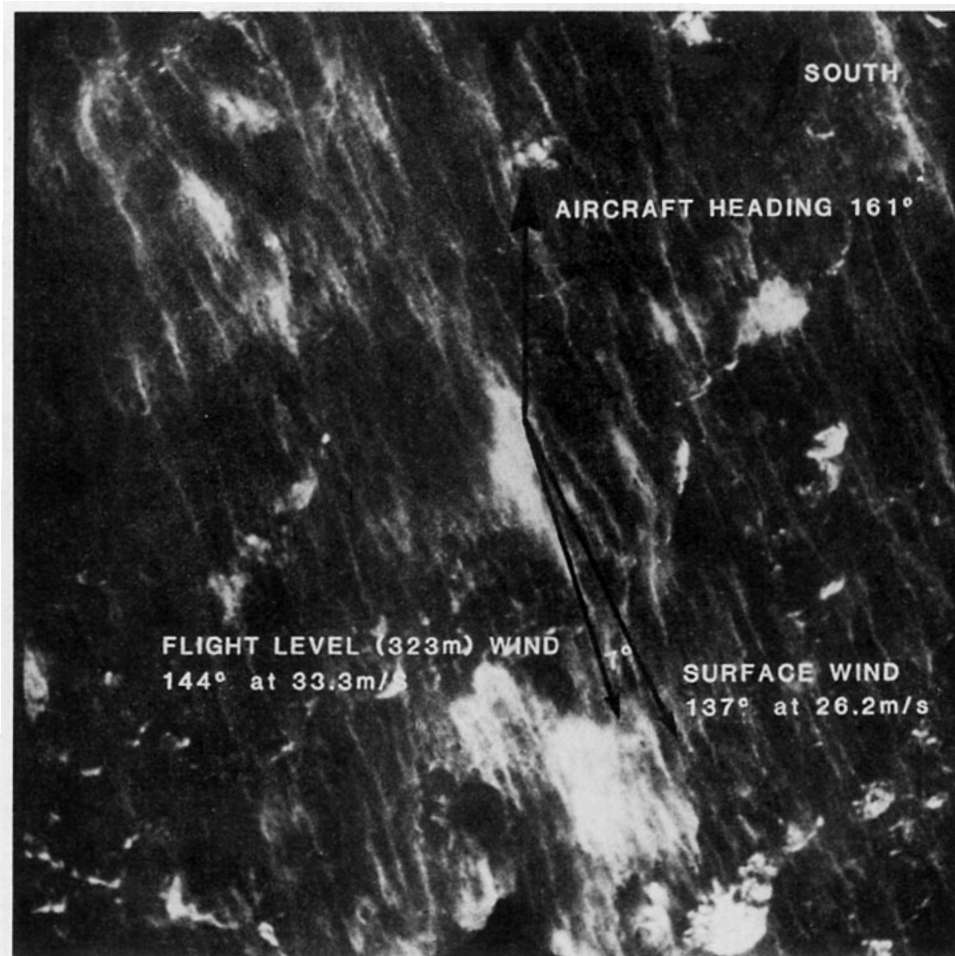
FIG. 5. Vertical camera photograph of the sea surface in Hurricane Eloise (1975). Foam streaks are parallel to the wind direction. A veering with height of 7° is indicated from the surface to 332 m.

2) LANDFALL ANALYSES

When the landfall observations were composited with respect to the storm center, land platform data could be found plotted adjacent to ocean platform data as shown in Fig. 3. This posed an analysis problem which was solved by preparing separate analyses for the ocean and land platforms respectively. We then merged the analyses by overlaying the coastal map for the storm position at the time that maximum winds were measured on the coast. The final analyses (Figs. 10 and 11) consisted of all the highest wind speed observations from land platforms over land and from sea-exposed platforms over water. These analyses are assumed to be representative of the storm at the time that most damage was occurring on the coast.

For the landfall composite, a few of the anemometer records were from stations with a water exposure. Dauphin Island Bridge (DPB) and University of Florida stations at Perdido Key (PDK) and Navarre (NVR) were on the east side of the landfall point and experienced onshore (PDK and NVR) or overwater

(DPB) flow. These stations were considered to be equivalent to over-water platforms. Wind direction data from these and other overwater platforms were used to adjust the aircraft directional data for veering with height of 10–20°.

g. Additional analyses

Radiosonde data, from Centreville, Alabama (CKL), and Jackson, Mississippi (JAN), for 1200 GMT 13 September were used for studying vertical wind structure in the vicinity of the storm over land.

Surface air temperatures were analyzed at landfall using available hourly observations over land (assumed to apply to the 10 m level) and determining temperatures over water by applying the boundary-layer model mentioned earlier to the aircraft data.

The wind damage in the storm was studied through a damage vector analysis made by Dr. Theodore Fujita of the University of Chicago. Fujita (1980) utilized his F-scale determinations to perform a damage vector analysis in Frederic as a part of the NHRL strike program. These damage vectors were related
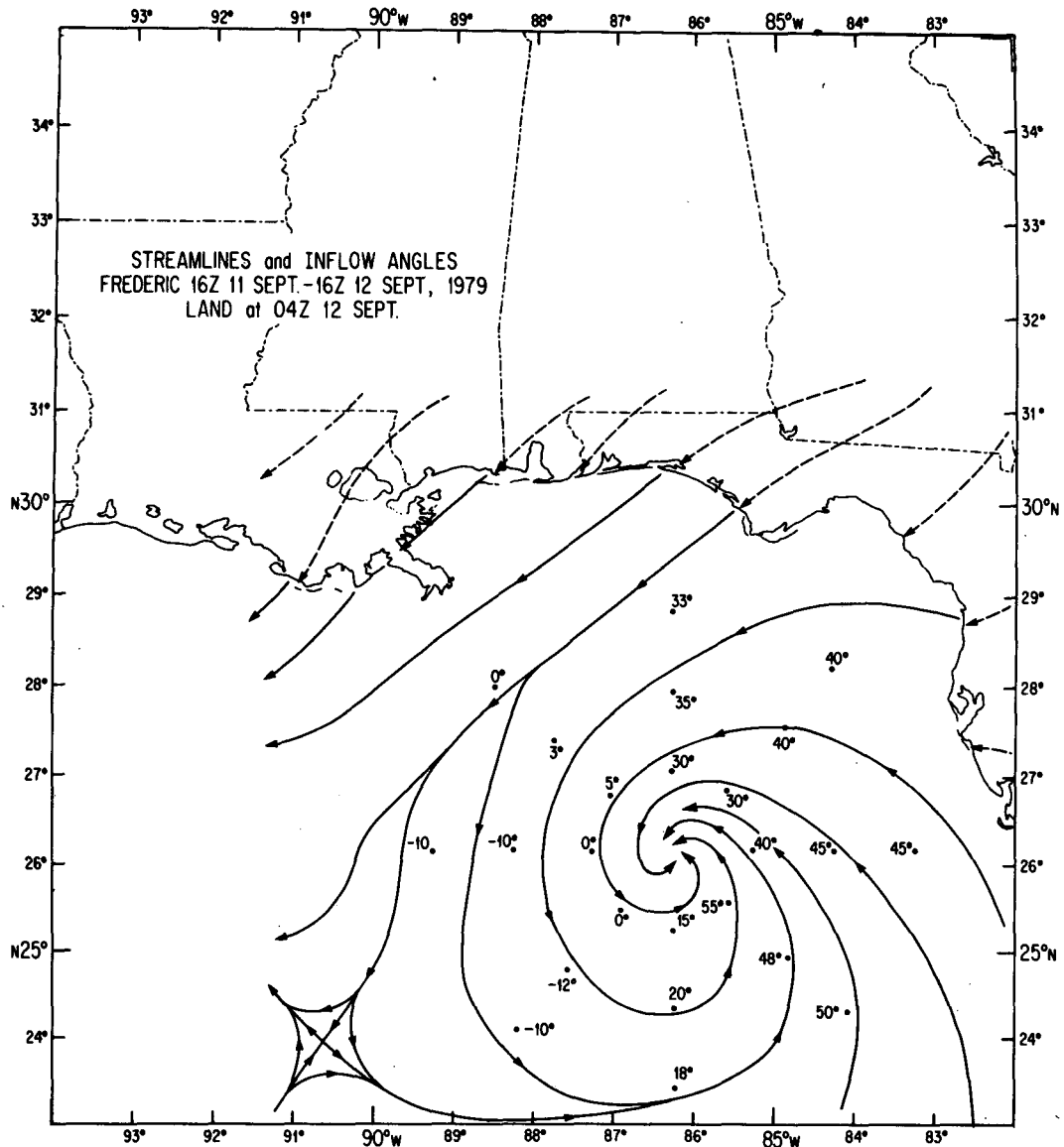
FIG. 6. Streamline analysis and inflow angles (degrees) for the overwater composite. Streamlines are dashed over land. Storm motion is 333° at 5 m s⁻¹.

to the surface wind field during the landfall composite.

4. Results

In this section the horizontal wind field is discussed in terms of probable physical influences and model wind fields. We relate aircraft measurements to land measurements. Aircraft and radiosonde data are used to study the vertical shear of the horizontal wind, and the wind field is related to the damage field.

a. The horizontal wind field and model comparison

The horizontal wind structure was determined from streamline and isotach analyses of the compos-

ited data for the overwater and landfall composite periods. The overwater composite streamline analysis and inflow angles (angle between the actual wind and a tangent to a circle passing through the data point centered at the storm) at 60 n mi (111 km) radii are presented in Fig. 6. Maximum inflow angles are observed in the southeast quadrant and maximum outflow angles are in the southwest quadrant. Fig 7 shows the isotach analysis for the same time period. A very large area of winds that are >15 m s⁻¹ is shown to extend northwest–southeast throughout the eastern Gulf of Mexico. The maximum wind speed of >40 m s⁻¹ is evident in the front right portion of the eyewall. An outer secondary wind maximum of 30 m s⁻¹ is ~135 km north-northwest from the storm center.
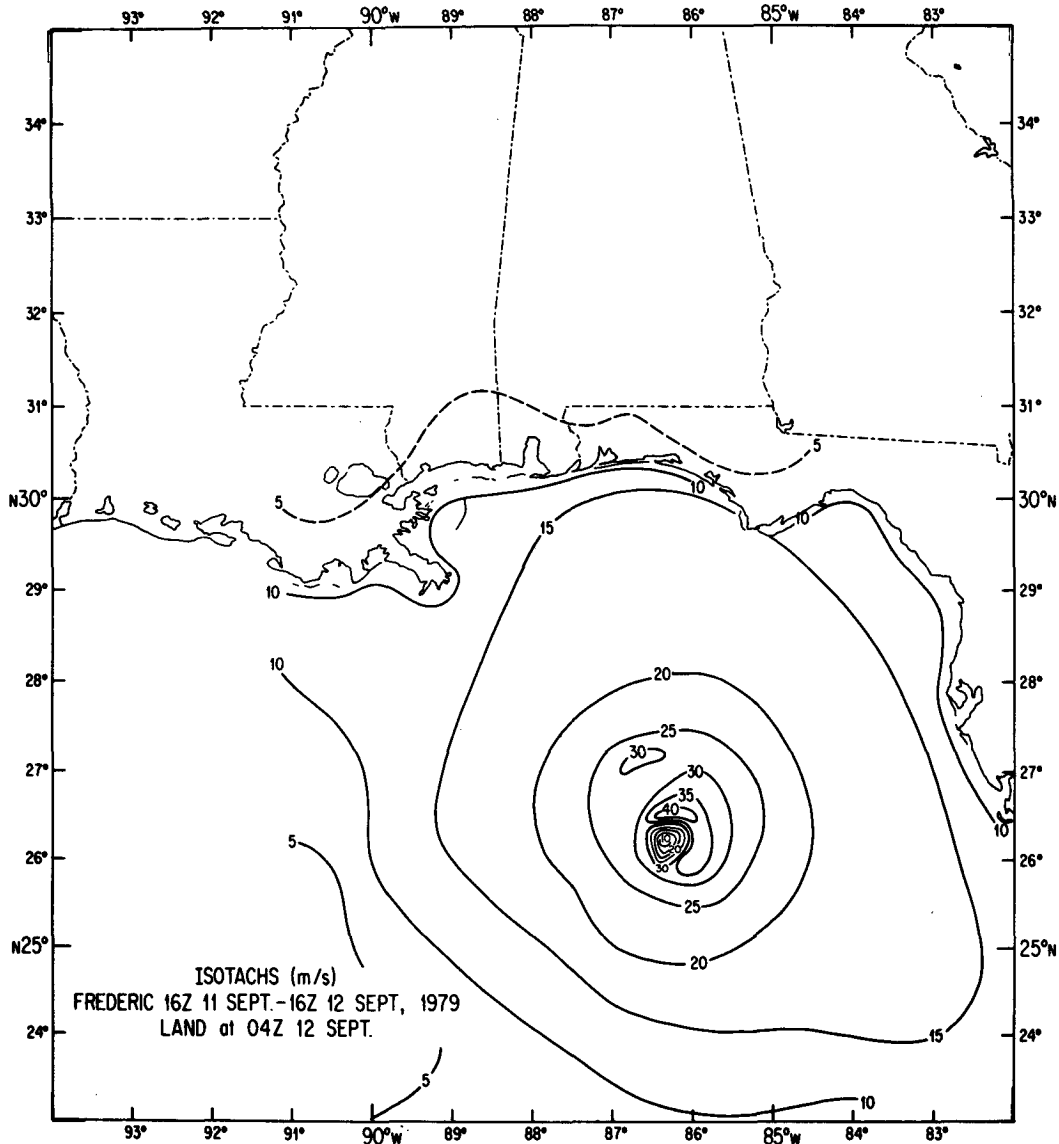
FIG. 7. Isotach analysis (m s^{-1}) for the overwater composite. Isotachs are dashed over land.
Storm motion is 330° at 5 m s^{-1}.

The secondary wind maximum was based on 500 m level aircraft measurements made by NOAA aircraft at 0012 GMT 12 September and 1140 GMT 12 September. The position of this feature is associated with an outer convective band of high [>40 dB(Z)] radar reflectivity in the PPI lower fuselage radar composite (Jorgensen, 1981) of Fig. 8. The radar composite may be compared with a smaller scale version of Figs. 6 and 7, which have been combined to give the isotach–streamline analysis on an approximate 300 × 300 km area centered on the storm at 0400 GMT 12 September 1979. This analysis is presented in Fig. 9. Willoughby *et al.* (1981) observed secondary wind maxima in intense, symmetric Hurricanes Anita of 1977, David of 1979 and Allen of 1980. He related the feature to a phenomenon in which an outer concentric convective ring propagates inward, eventually becoming part of a "double eye" structure and finally displacing the original eye. Frederic was an asymmetric storm and no propagation of the secondary wind maximum relative to the storm center was observed during the 12 h period between aircraft measurements.

For the landfall composite, the streamline and inflow angle analysis in Fig. 10 indicates that maximum inflow angles, at landfall, were in the northeast quadrant, with minimum inflow angles in the southwest. It is well known that flow, experiencing a change in roughness from smooth to rough, is decelerated. The decrease in speed reduces the outward-directed Coriolis and centrifugal force components and allows the inward directed pressure gradient force to accel-

FREDERIC 790912H1 LF 1.5km
Domain: 300X360 km N= 39 Thresh(dBz)=25.,30.,35.,40.,
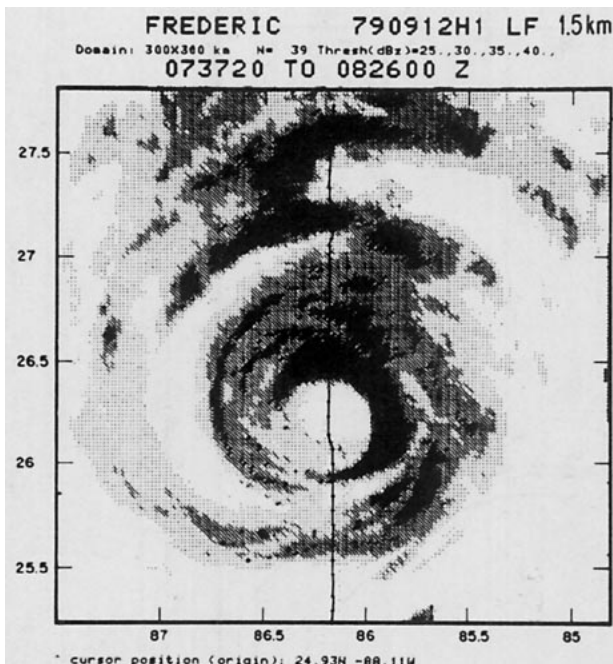073720 TO 082600 Z

FIG. 8. Airborne lower fuselage radar PPI composite pertaining to Fig. 9 for 12 September 0737 to 0826 GMT. Four reflectivity levels [dB(Z)] are enhanced (from Jorgenson, 1981). Storm motion is 330° at 5 m s^{-1}.

erate the flow farther inward. The movement of the position of the maximum inflow angles from the southeast in the overwater composite to the northeast in the landfall composite is in accordance with a roughness change from the sea surface to land terrain. The isotach analysis for the landfall composite is presented in Fig. 11, and indicates that there was a large change in the 10 m level wind structure at the coastline. The area of maximum wind speed > 45 m s^{-1} can still be seen in the right front portion of the eyewall, and a wind maximum of 35 m s^{-1} is shown to occur in the left eyewall. There is no evidence of an outer secondary wind maximum. Note that the area of winds >15 m s^{-1} is much smaller than in Fig. 7.

The discontinuities shown in the landfall streamline and isotach analyses are indicative of the change in terrain roughness at the coastline. As stated earlier, over-land flow is characterized by larger inflow angles. The surface terrain obstacles over land extract energy from the flow (friction), increasing the level of turbulence and decreasing the speed. The overland wind speed measurements were consistently lower than adjacent overwater measurements, resulting in an analysis with an abrupt speed change that coincided with the terrain change at the coast.

Table 1 shows a comparison of the wind speed from the analysis at successive distances west (negative distance) and east (positive distance) from the landfall point, over the land and over the water ad-

jacent to the coast. The distances between the overland and over-water locations relative to the coast were minimized, and are thought to be representative of a 10 km separation. The ratio of overland to overwater wind speeds for onshore flow on the right side varies from 0.74 to 0.84, which is slightly lower than the value of 0.89 determined by Myers (1954) for the ratio of off-water measured winds to overwater winds in the 1949 and 1950 hurricanes at Lake Okeechobee, Florida. The average ratio of coastal overland to overwater winds for offshore flow in Myers' study varies with wind speed and is included in Table 1 for comparison.

The mean ratio of overland V_L to over-water V_0 winds in Frederic was 0.8. This value is important because it relates V_L to V_0, and V_0 is related to the flight level wind V_a through the boundary-layer model. This is discussed in more detail in Section 4b.

It is instructive at this point to compare the model-generated surface wind field of Moss and Jones (1978) at the time of maximum coastal winds (Fig. 12) with the Frederic composite analysis at the time of maximum winds at the Dauphin Island Bridge. The Frederic analyses of Figs. 10 and 11 were combined and enlarged to Fig. 13 to facilitate comparison. In addition, an aircraft lower fuselage radar PPI composite from 0100 to 0300 GMT 13 September is provided in Fig. 14. The scale is approximately the same as that of Figs. 8, 9, 12 and 13. Some basic differences between the model and composite analyses should be
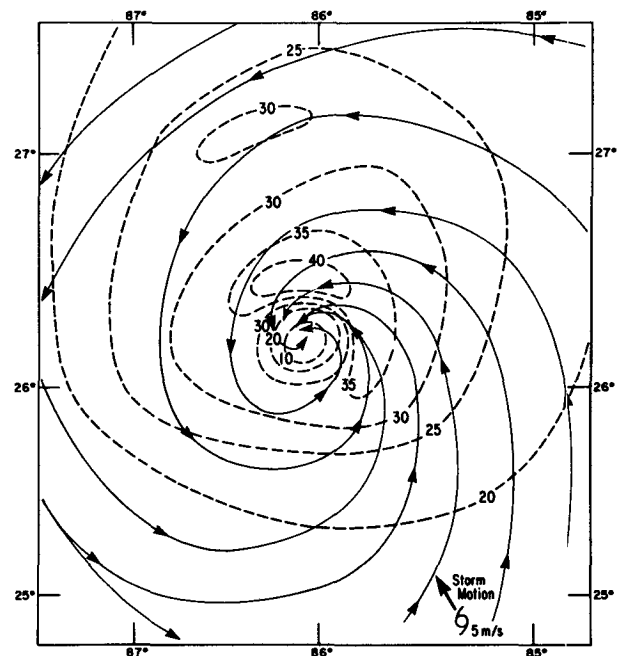

FIG. 9. Combined isotach (m s^{-1})–streamline analysis for the over-water composite pertaining to Figs. 6 and 7 on an area of approximately 300 × 300 km. Arrow in lower right corner depicts storm motion to the northwest at 5 m s^{-1}.

kept in mind before comparison. The lower model level for surface wind computations is a sigma coordinate surface which is actually well above the surface (~500 m), although model physics treat it as the earths surface. Another point is that the model storm is in the process of losing intensity with the central pressure rising from 940 to 982 mb in the ten hours previous to landfall while Frederic was in a relative steady state preceding landfall.

Several features of the observed wind field and the model field may be emphasized:

1) The maximum model confluence is in the landward front right quadrant and minimum confluence is on the left side near the coast in Fig. 12; these features compare favorably with the inflow angles and confluence at the coast in the composite analyses of Figs. 10 and 13.

2) The maximum coastal wind speed locations are both in the front right quadrant of the storm.

3) Both the composite analysis and the model indicate discontinuities of wind speed at the coast, although the model discontinuity is weak.

4) The Moss–Jones study indicates a rotation of the wind speed maximum from the right to the front of the storm, in response to increased inflow leading to a stronger radial pressure gradient over land. The Frederic case indicates that the wind speed maximum persisted in the right front quadrant of the eyewall during both composites. The right front quadrant
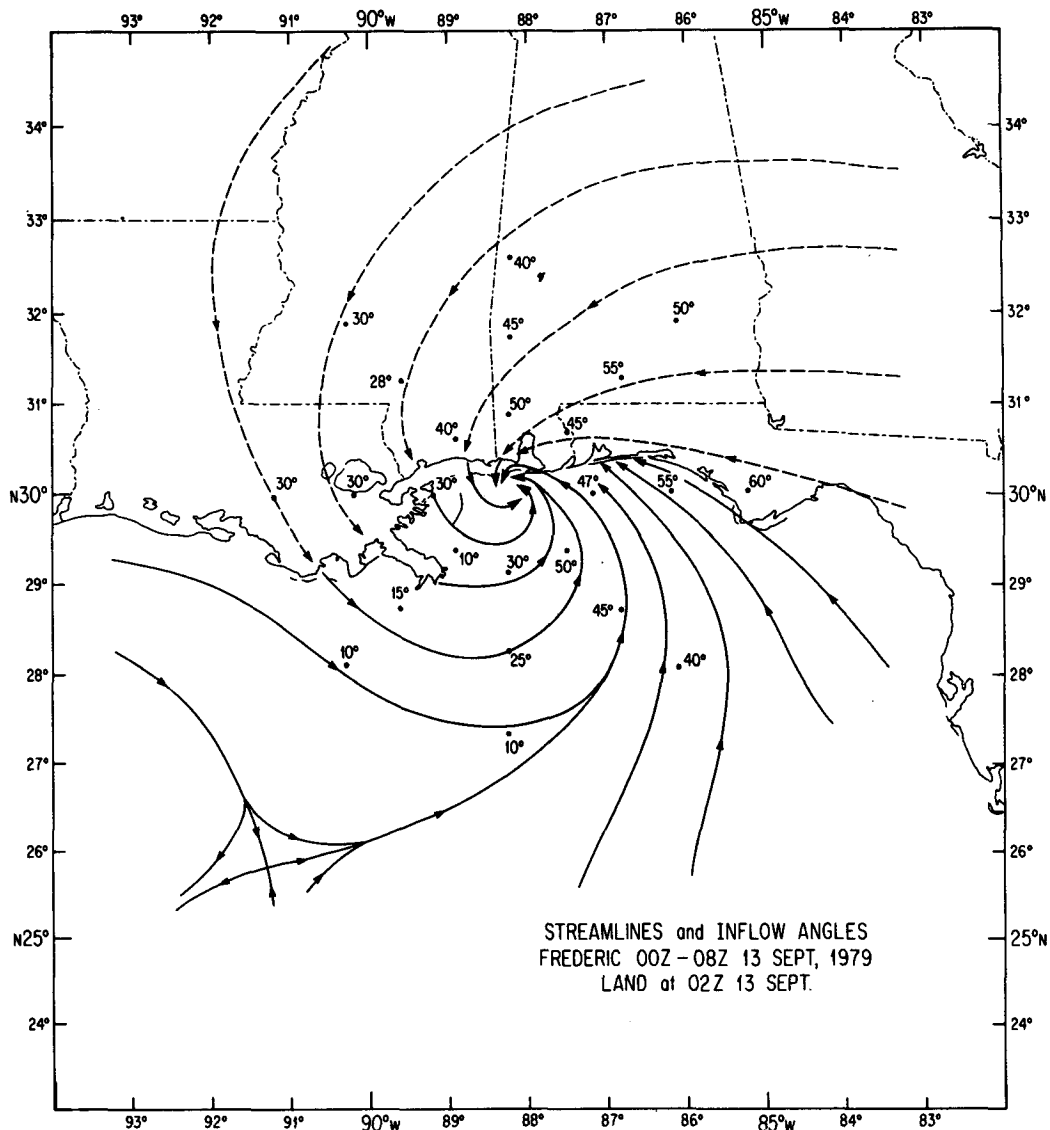

FIG. 10. Streamline analysis and inflow angles (degrees) for the landfall composite. Streamlines are dashed over land. Storm motion is 345° at 6.5 m s⁻¹.
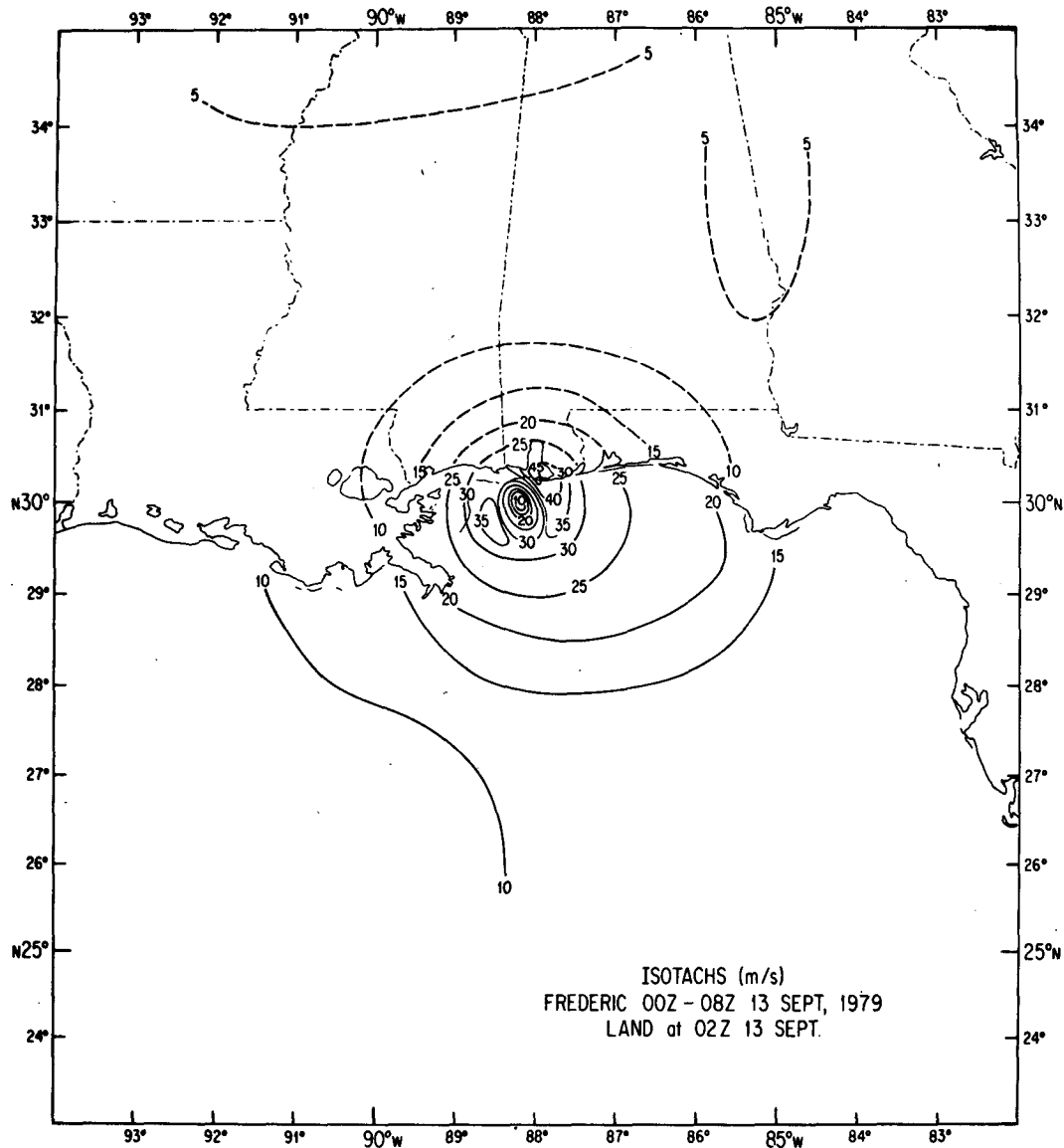
FIG. 11. Isotach analysis (m s⁻¹) for the landfall composite. Isotachs are dashed over land.
Storm motion is 345° at 6.5 m s⁻¹.

coincides with the area of maximum inflow angle in Fig. 10.

5) The region of strongest coastal winds in the model field is associated with a maximum vertical motion of 6 m s⁻¹ at the top of the boundary layer. The coastal wind maximum area in Frederic was associated with a radar reflectivity of >40 dB(Z) in Fig. 14.

6) Although both the model and the observations indicate a wind maximum associated with the eyewall to the southwest, the model shows significant confluence, and the observations on the southwest side show little confluence. The southwest side of Frederic was associated with minimum inflow angles during both composites and is related to a surrounding easterly environmental flow, while the model study involved a southerly environmental steering current. The environmental flow would act to increase inflow upwind of the storm center and decrease inflow downwind of the storm center.

7) The ratio of model overland to overwater wind speeds adjacent to the coast is included in Table 1. The distance between overland and over-water locations is 20 km (two grid intervals) and the mean ratio is larger than that in the Frederic study. The mean model ratio is ~0.9 as opposed to 0.8 for Frederic, and is probably sensitive to the drag coefficient used to parameterize the land terrain.

Tuleya and Kurihara (1978) also carried out a model landfall experiment. Although analyses at the time of maximum winds on the coast were unavail-

TABLE 1. Ratio of overland wind speed V_L to overwater wind speed V_0 at coast for 8 h composite at 0200 GMT land position in Frederic, Moss–Jones (1978) model, and Lake Okeechobee studies.

	Radial distance from landfall point (km)										Mean ratios
	−150	−115	−80	−45	−10	25	65	100	140	175	
Overland wind speed, V_L (m s^{-1})	13	16	21	26	27	35	33	24	22	17.5	
Over-water wind speed, V_0 (m s^{-1})	17	21	24	31	33	45	41	30	26	23.5	
Ratio (Frederic) (5–10 km separation)	0.76	0.76	0.87	0.83	0.81	0.77	0.78	0.8	0.84	0.74	0.796
Ratio (model) (20 km separation)	0.86	0.93	1.0	1.0	0.69	1.0	0.86	0.93	0.90	—	0.907
Ratio (Myers, 1954b) (Lake Okeechobee)	0.52	0.58	0.60	0.69	0.71	0.89	0.89	0.89	0.89	0.89	0.755

able from the Tuleya and Kurihara experiment, features that compare well with the Frederic observations and the Moss and Jones experiment deserve comment. At landfall, the winds over land are much less than those over water. Maximum vertical motion in the model is located directly in front of the center. Maximum convergence is located from the center to the right along the coastline and maximum divergence is positioned along the coast to the left of the center.

Although many features of the model wind fields compare well with the Frederic landfall wind field, it appears that individual comparisons of several intense landfalling hurricanes would be required to fully verify the model results. An experiment is being planned to employ a model with higher Planetary Boundary Layer (PBL) resolution and resolvable-scale convection to repeat the Moss–Jones study and verify the model results.

It is apparent from the above comparisons that the actual deceleration of onshore winds and acceleration of offshore winds at landfall is substantial and is caused by the change in roughness experienced by the flow.

b. Estimation of coastal surface wind gusts from low-level aircraft winds

When hurricanes are making landfall, Air Force and NOAA reconnaissance aircraft are unable to penetrate the storm or fly over land because of the danger of added mechanical and convective turbulence and the possibility of tornadoes. Once the hurricane nears land, the aircraft continue to provide information to the National Hurricane Center by flying parallel to the coast in what is known as a "strike mode."

The hurricane forecaster has aircraft-measured wind data in the high wind region of the storm before landfall at his disposal and uses this information, plus other available data, and his experience to issue warnings and advisories. It would be helpful to have readily usable relationships to enable the forecaster to estimate coastal mean winds and peak gusts based on

aircraft data measured earlier in the same relative positions in the storm. It was possible to employ the Frederic landfall composite aircraft and coastal data to construct such relationships.

The results from the previous section and Table 1 indicate that the overland 10 m level wind (V_L), adjacent to the coast, is approximately 80% of the over-water 10 m level wind (V_0) just offshore. V_0 is currently estimated for research purposes through use of a diagnostic boundary-layer model (Powell, 1980). The ratio of model-computed V_0 to aircraft-measured wind speed V_a (at altitudes ranging from 500 to 1500 m) varies with stability and wind speed from ~0.6 to 0.8 in stable and unstable conditions, respectively,
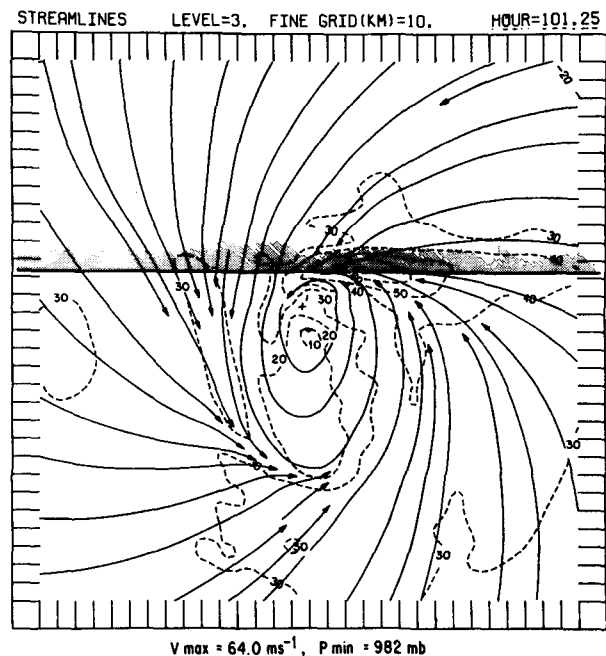

STREAMLINES   LEVEL=3.   FINE GRID(KM)=10.   HOUR=101.25

V max = 64.0 ms^{-1}, P min = 982 mb

FIG. 12. Model landfall experiment streamline and isotach analysis (m s^{-1}). Tick marks are at 10 km intervals and area is 300 × 300 km. (from Moss and Jones, 1978). Storm motion is 360° at 4 m s^{-1} and the coastline is denoted by a solid straight line adjacent to the shaded area.
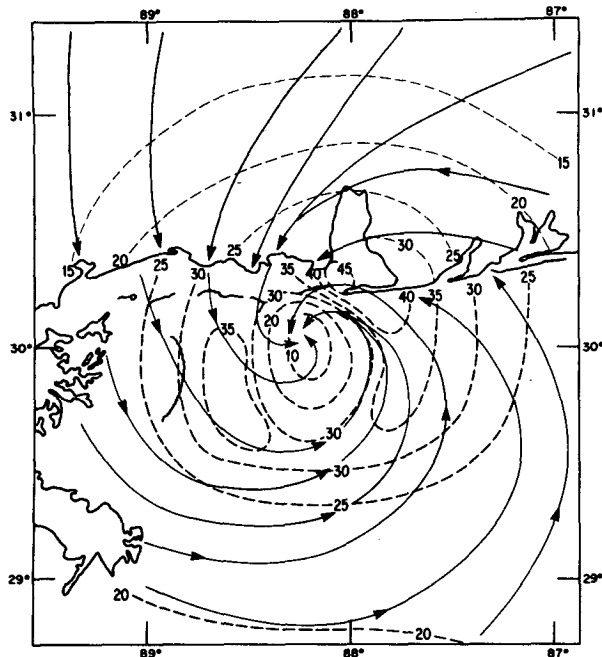
FIG. 13. Combined isotach–streamline analysis for the landfall composite pertaining to Figs. 10 and 11 on an area of approximately 300 × 300 km.

for the wind speed range of 25–50 m s^{-1}. Limited comparisons of buoy-measured mean winds with mean aircraft winds in Hurricanes Eloise and Anita indicate a ratio of 0.7 for winds >20 m s^{-1}. Hence, the value of 0.7 seems appropriate for V_0/V_a.

In the Frederic landfall composite, 10 of the hourly coastal land observations, plotted with respect to the storm center, were within 5 km of aircraft observations, which were also plotted relative to the storm. Thus, it was possible to compare coastal winds with previously measured aircraft winds. Time differences between observations ranged from twelve minutes to almost four hours. Coastal data from Ingalls Shipyard in Pascagoula, Mississippi, Pensacola Naval Air Station (NPA) and Pensacola Regional Airport (PNS) consisted of anemometer charts from which it was possible to deduce a 5–10 min mean wind and a peak gust over a 10 min period centered on the hour. Gust data were adjusted to the 10 m level with a power law as applied by Atkinson and Holliday (1977). Coastal data from Keesler Air Force Base (KSL) in Biloxi, Mississippi, consisted of mean and peak gusts taken from the observations log and correspond to a 1 min period. The aircraft mean winds are 30 s averages and are equivalent to a storm sample distance of 3 km. A 5–10 min average corresponds to a sampling distance of 2–4 km at a storm speed of 6.5 m s^{-1} and a 1 min average corresponds to a 0.4 km sample distance. As stated in Section 3, the wind data from the various averaging periods showed no systematic differences in the composite plots, but the 1 min wind speeds may be slightly greater than the

5–10 min wind speeds. The peak gust during 1 min at KSL could be different from a 10 min gust, but is representative of gust conditions occurring over longer time periods.

The wind speed data, ratios and gust factors are presented in Table 2. The gust factor G is defined as the ratio of the peak gust V_{LG} to the mean wind V_L during a specified averaging period (here corresponding to 10 min). Gust factors from stations on the west side of the landfall point, in north winds, are higher than those on the east side in south winds, indicating different terrain and fetch-dependent turbulence levels. The mean V_L/V_0 and V_0/V_a ratios of 0.81 and 0.71 compare well with the previously mentioned results of 0.8 and 0.7. The mean ratio of the overland peak gust to the aircraft mean wind was 0.8. Miller (1964) compared the surface to 900 mb level mean layer rawinsonde wind speeds to the peak gusts measured by gust recorders at the rawin stations during the release hour in Hurricane Donna. He found a ratio of mean-layer wind speed to peak gusts of 0.85 to 0.9. His larger ratios would be expected because:

1) The mean surface-to-900 mb layer wind is probably less than what an aircraft would measure at 500 m over water.

2) The peak gust over an hour is probably larger than one over a 10 min period.

3) A gust over land would be a higher percentage of the wind directly above because of stronger turbulent mixing.

The mean ratio of V_L/V_a in Frederic was 0.58. The ratio of V_L/V_a may also be determined from

$$\frac{V_L}{V_a} = \frac{0.8 V_0}{V_a} = \frac{0.8(0.7 V_a)}{V_a} = 0.56. \qquad (2)$$

The ratio of V_{LG}/V_a may be combined with the above V_L/V_a to estimate a coastal station gust factor G:

$$G = \frac{V_{LG}}{V_L} = \frac{0.8 V_a}{0.56 V_a} = 1.43. \qquad (3)$$

This compares well with the mean gust factor of 1.42 computed from the coastal stations with 10 min gusts and also with the findings of Atkinson (1974) for 10 min averages at coastal sites for onshore flow. Atkinson's gust factors varied from 1.40 to 1.45.

Although more coastal and offshore aircraft data are required to fully establish the above relationships, they may be useful aids to forecasters preparing warnings and advisories with aircraft-measured wind speed data as guidance.

c. The vertical shear of the horizontal wind

The strong frictional decrease of surface winds before landfall indicated in Fig. 13 and Table 1 has implications for the vertical structure of the horizontal winds. One would expect stronger mechanical mixing and mechanically produced wind shear due

to larger roughness elements over land and strong convective scale vertical motions in the region of convergence at the coastline. Although vertical motions have not been computed in this study, their existence is indicated in the radar depiction of Fig. 14, and in radar investigations of Frederic by Parrish *et al.* (1982).

The vertical wind structure, determined by radiosonde data from Jackson, Mississippi (JAN) and Centreville, Alabama (CKL) (see Fig. 1), was studied in terms of the vertical shear of the horizontal wind speed, as shown in Table 3. Shears at the land stations at 1200 GMT 13 September were compared with shear determined from aircraft-measured 500 m winds and 10 m level model-computed winds over water in the same position relative to the storm center for the over-water composite period.

Mechanical wind shear is produced when surface air, slowed by friction with the terrain, lies below high wind speed flow that is unimpeded by obstacles. Comparison of over water and overland speeds in Table 3 indicates that 500 m level winds over water and land did not differ appreciably, but 10 m level winds over land were much lower than over water. It is apparent that the wind speed shear is stronger over land, even at 8 h after landfall, and appears to be mechanically produced. Wind shear was also estimated at the Dauphin Island Bridge (DPB) southeast of the center of the storm, by using the 10 m level wind in conjunction with a 500 m level aircraft-measured wind in the same relative position 4 h earlier. The wind shear at the bridge, which had an over-water exposure, was similar, in magnitude to that computed in the same relative position for the over water composite period, indicating that shear may be comparable near the core of the storm before and during landfall.

Although the most likely mechanism for the observed wind shear is the frictional retardation of surface flow caused by land roughness elements, another mechanism was investigated. During landfall, the airflow over land is subject to cooling without the augmentation of surface heat and moisture fluxes from the sea. Adiabatic inflow, precipitation downdrafts and evaporation are all possible cooling processes. The 10 m level composite temperature field for Frederic at landfall in Fig. 15 indicates a cold core in the surface circulation centered on the central Mississippi coast. If we assume a near-stationary storm, i.e., a trajectory approximates a streamline, the temperature decrease along a streamline from the Pensacola area to the center of the cold core of 4°C corresponds to a pressure decrease from 988 to 950 mb. The dry adiabatic cooling associated with such a pressure decrease is 3.5°C. Therefore, it appears that adiabatic cooling at landfall could be the primary cause of the development of a cold core of surface air. The observed cold core in the surface temperature field compares well with the composite analysis of United
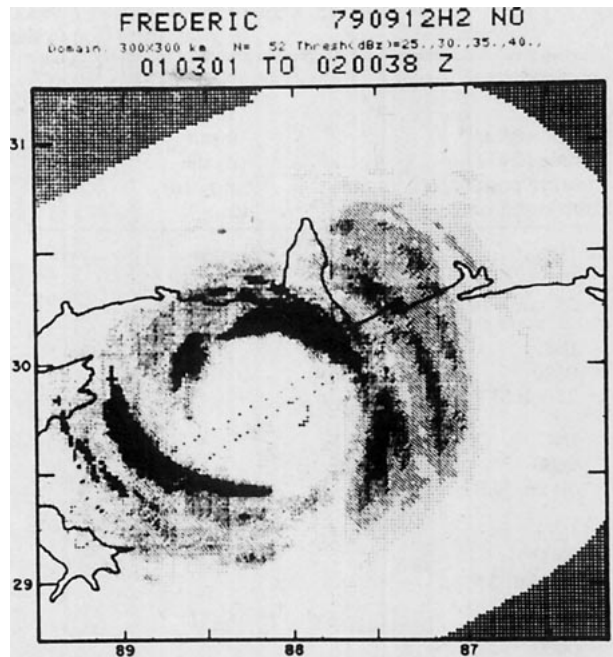

FIG. 14. Airborne nose radar PPI composite pertaining to Fig. 13, for 0103–0200 GMT 13 September.

States hurricanes with tornadoes by Novlan and Gray (1974). Both indicate the cold core in the left front quadrant of the storm.

The horizontal temperature gradient associated with this cold core was investigated as a possible mechanism for producing vertical shear of the horizontal wind according to the "thermal wind" concept

$$\frac{\partial V}{\partial z} = \frac{1}{[2v/(r+f)]}\left[\frac{R}{P}\frac{\partial T}{\partial z}\frac{\partial p}{\partial r}\bigg|_z + \frac{g}{T}\frac{\partial T}{\partial r}\bigg|_z\right]. \quad (4)$$

This equation pertains to the vertical shear of the tangential gradient wind component V, where r is the radius from the storm center, f is the Coriolis parameter, R is the gas constant for dry air, p is the gradient level pressure, T is temperature, g is the gravitational acceleration and z is height. This equation was evaluated on the assumption of a 500 m gradient wind level, neutral stability and 500 m horizontal temperature and pressure gradients equivalent to those observed at the surface. As seen in Table 3, the thermal wind shear is insignificant, even close to the core of the hurricane.

d. Relationship of the wind field to the damage field

The surface wind field, as shown in Fig. 13, has gusts superimposed on it. Surface gusts are produced by mechanical and convective transports of momentum downward augmented by evaporation-cooled air in precipitation downdrafts and the local mesoscale pressure gradient. These gusts were responsible for most of the damage determined by Fujita (1980) in

TABLE 2. Ratio of the 10 m level overwater wind (V_0), overland wind (V_L), and overland peak gust (V_{LG}) to the low-level aircraft wind (V_a).

Land station;* time (GMT); relative position from storm center	Aircraft time (GMT)**	V_0 30 s 10 m mean (model computed) (m s^{-1})	V_a 30 s mean wind (m s^{-1})	V_L 10 m mean land (m s^{-1})	V_{LG} 10 m land gust	$\dfrac{V_0}{V_a}$	$\dfrac{V_L}{V_0}$	$\dfrac{V_L}{V_a}$	$\dfrac{V_{LG}}{V_a}$	Gust factor $G = \dfrac{V_{LG}}{V_L}$
ING 0300 25 km NW	42RF 0016	31.0	47.0	28.9	43.4	0.66	0.93	0.61	0.91	1.50
ING 0500 25 km SSW	42RF 0212	20.2	25.9	11.3	18.8	0.78	0.56	0.44	0.71	1.66
ING 0600 50 km SSE	42RF 0216	33.7	48.0	22.2	35.0	0.70	0.66	0.46	0.72	1.58
ING 0800 120 km S	43RF 0710	25.7	35.1	18.6	28.7	0.73	0.72	0.53	0.82	1.54
NPA 0600 150 km ESE	42RF 0337	24.9	33.0	24.0	28.8	0.75	0.96	0.73	0.92	1.20
NPA 0700 170 km SE	43RF 0650	22.4	33.6	22.7	29.3	0.66	1.01	0.67	0.92	1.29
NPA 0800 195 km SE	42RF 0442	23.5	31.2	21.6	27.4	0.75	0.92	0.69	0.92	1.27
KSL 0500 50 km W	42RF 0135	34.5	49.5	30.2	38.3	0.70	0.87	0.61	0.73	1.26
KSL 0600 50 km SW	42RF 0114	37.2	54.0	27.2	35.5	0.69	0.73	0.50	0.62	1.30
PNS 0700 170 km SE	43RF 0648	22.5	32.1	17.5	23.7	0.70	0.77	0.54	0.72	1.35
Mean ratios						0.71	0.81	0.58	0.80	1.39 (1.42 excluding KSL)

* ING = Ingalls Shipyard, Pascagoula, MS; NPA = Pensacola Naval Air Station; PNS = Pensacola Regional Airport; KSL = Keesler Air Force Base, Biloxi, MS.
** 42RF = NOAA P3 No. 42; 43RF = NOAA P3 No. 43.

his damage analysis of Hurricane Frederic. Fujita categorized the damage according to the wind speed ranges that were required to produce the damage as $F0$, $F1$ or $F2$. These F scales correspond to mean wind speed ranges of 18–25, 26–35 and 36–48 m s^{-1}, respectively. This correspondence is according to the conversion (Fujita, 1971) from F scale to mean wind speed. Most of the severe $F2$ damage occurred in the northern eyewall of the storm, before the landfall of the storm center. The damage at the three locations was associated with areas of intense radar reflectivity associated with the northern eyewall from 0022 to

0400 GMT, 13 September. The aircraft nose radar PPI composite in Fig. 14 shows an area of >45 dB(Z) reflectivity associated with the northern eyewall. This indicates that the gusts producing the damage could have been associated with convective transfer of momentum downward, causing winds from the level of strongest wind speed (500–1500 m) to be transported to the surface. Eyewall downdrafts were strongest at this level and the winds at this level still had significant inflow (Jorgensen, 1981). Therefore, it is conceivable that surface gusts from such downdrafts could have caused $F1$ and $F2$ damage and that the

TABLE 3. Frederic vertical wind shear.

Station and time (GMT)	Radius and azimuth	500 m level wind speed (m s^{-1})	10 m wind speed (m s^{-1})	Horizontal temperature gradient [°C (100 km)$^{-1}$]	Total vertical wind shear (s^{-1})	Thermal wind shear (s^{-1})
JAN						
13 September 1200	155 km W	26.5	8.2	1.0	3.7 × 10^{-2}	0.023 × 10^{-2}
Over water						
11 September 2300	155 km W	25.0	17.0	—	1.6 × 10^{-2}	—
CKL						
13 September 1300	189 km NE	27.8	9.3	1.1	3.8 × 10^{-2}	−0.34 × 10^{-2}
Over water						
12 September 1200	189 km NE	33.0	23.0	—	2.0 × 10^{-2}	—
DPB						
13 September 1300	33 km ESE	47.7*	28.0	2.0	4.0 × 10^{-2}	−0.03 × 10^{-2}
Over water						
12 September 1200	33 km ESE	52.0	35.0	—	3.4 × 10^{-2}	—

* 500 m wind maximum was measured by aircraft at 0008 GMT in same relative position.
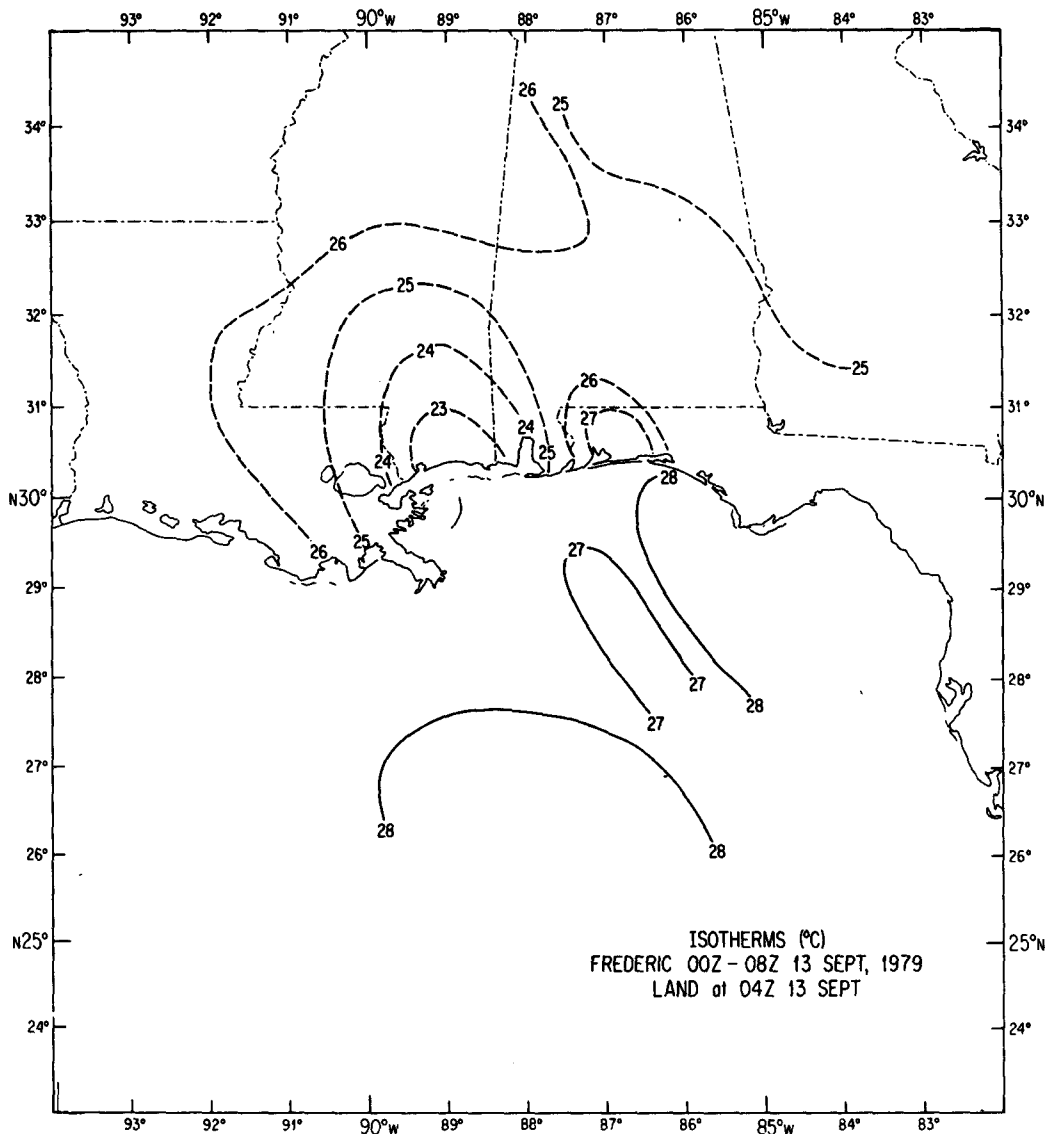
FIG. 15. Ten-meter-level landfall composite temperature field (°C).
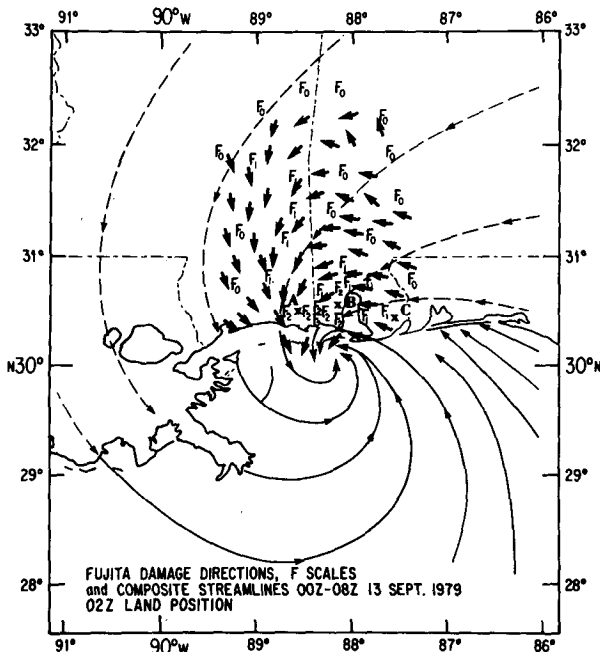
FIG. 16. Fujita damage vector directions, damage scales and streamlines from landfall composite.

damage directions would be correlated with the surface wind directions. By advancing the analysis in Fig. 13 along the storm track and comparing damage direction vectors with the 10 m level streamline directions, we found that the damage vectors were well correlated with the 10 m wind directions. By assuming the damage-causing gusts were in the same direction (aligned to within 5°) as the 10 m wind field, it was possible to estimate the time period during which the damage occurred and the mean wind speed range that produced the damage. Fig. 16 shows the streamline analysis and F scale damage directions at 0200 GMT, 13 September.

Three locations were studied that correspond to points A, B and C on Fig. 16 and Table 4. At Pascagoula (point A), just to the west of the landfall point, the wind persisted from the north for 4.5 h, whereas south of Mobile (point B) and at Foley (point C), the damage directions aligned with the wind directions for 0.75 and 1.5 h, respectively. These short damage time intervals could have consisted of damage primarily by eyewall gusts, whereas the 4.5 h period of A may also have contained fatigue damage from sustained high winds from the north. Wind directions in the northwest quadrant of Frederic during the landfall composite were observed to vary less in time than directions in the other quadrants.

The mean wind speed ranges in Table 4 for points A, B and C contain the maximum mean wind experienced at the respective locations during the landfall according to the converted F-scale range. It is possible that the data coverage over land was not suf-

ficient to completely resolve the maximum wind speed region of the northern eyewall, or that the Fujita scale requires further calibration. Golden (1976) compared F-scale wind speed estimates to engineering and photogrammetric techniques in the Xenia, Ohio, tornado of 1974 and found comparable wind speed magnitudes and ranges for $F2$ to $F3$ damages. Similar calibration of the F scale versus the above methods and wind speed observations would be desirable in hurricanes.

5. Conclusions

The low-level wind structure of Hurricane Frederic, as studied through composite analysis, reveals several features that are summarized below:

1) A low-level secondary wind maximum associated with an outer convective band was observed in the overwater composite analysis.

2) The effect of the landfall process is to shift the region of maximum inflow angle from the right rear portion of the storm to the landward side.

3) The frictional effect causes mean winds immediately inland from the coast to be 20% less than mean winds immediately offshore.

4) The landfall composite analysis compared well with model landfall experiment analyses in the position of the wind speed maxima and confluence and in the occurrence of discontinuities at the coastline.

5) Ten-meter-level gusts at coastal stations may be estimated as 80% of the low-level aircraft mean winds measured previously in the same relative location with respect to the storm. The 10 m level mean wind at coastal stations is only 56% of the low-level aircraft mean wind.

6) A good estimate of the coastal gust factor is 1.4 for 10 min mean winds at the 10 m level.

7) The vertical shear of the horizontal wind speed is greater over land than over water and is most likely caused by increased surface friction. Thermal wind

TABLE 4. Relationship of F scale to wind field.*

Location	F-scale damage and direction		Time interval (GMT) of alignment of mean wind with damage vector	Mean wind speed range during time interval (m s^{-1})
A (NW of Pasagoula, MS)	$F2$	011°	0000–0430 $T_L - 4$ to $T_L + \frac{1}{2}$	16–33
B (S of Mobile, AL)	$F2$	051°	0200–0245 $T_L - 2$ to $T_L - 1$	27–31
C (Foley, AL)	$F1$	120°	0230–0400 $T_L - 1.5$ to T_L	24–26

* T_L = time of landfall of center = 0400 GMT; $F0$ = 18–25 m s^{-1}; $F1$ = 26–35 m s^{-1}; $F2$ = 36–48 m s^{-1}.

calculations indicated that any thermal effects are negligible in producing wind shear.

8) A cold core to the west of the storm center was observed in the 10 m level temperature field at landfall which is probably due to adiabatic cooling.

9) A composite analysis and Fujita damage vector analysis may be used to determine the time interval during which the damage occurred, and the mean wind speed range, during the time interval. The mean winds from the composite analysis were less than the wind speeds determined from F-scale conversions.

10) The damage time intervals at the three locations revealed periods as short as 0.75 h, presumably when gust-related damage occurred, and as long as 4.5 h, when both gust and sustained wind damage took place. Most of the severe damage occurred in the northern eyewall, before the landfall of the storm center, and was probably associated with convective downward transport of momentum from higher levels.

REFERENCES

Atkinson, G. D., 1974: Investigation of gust factors in tropical cyclones. U.S. Fleet Weather Central Tech. Note JTWC

74-1, 9 pp. [Box 12 COMNAVMARIANAS F.P.O. San Francisco, CA 96630].

——, and C. R. Holliday, 1977: Tropical cyclone minimum sea level pressure/maximum sustained wind relationship for the western North Pacific. *Mon. Wea. Rev.*, **105**, 421–427.

Black, P. G., 1972: Some observations from hurricane reconnaissance aircraft of sea-surface cooling produced by Hurricane Ginger (1971). *Mar. Wea. Log*, **16**, 288–293.

Bradbury, D. L., 1971: The filling over land of Hurricane Camille, August 17–18, 1969. SMRP Res. Pap. No. 96, Dept. Geophys. Sci., University of Chicago, 25 pp.

Chow, S., 1971: A study of the wind field in the planetary boundary layer of a moving tropical cyclone. M.S. thesis, Dept. Meteor. Oceanogr., New York University, 59 pp. [NHRL Library, Coral Gables, FL 33146].

Durst, C. S., 1960: Wind speeds over short periods of time. *Meteor. Mag.*, **89**, 181–186.

Fujita, T. T., 1971: Proposed characterization of tornadoes and hurricanes by area and intensity. SMRP Res. Pap. No. 91, Dept. of Geophys. Sci., University of Chicago, 42 pp.

——, 1980: In search of mesoscale windfields in landfalling hurricanes. *Preprints, 13th Tech. Conf. on Hurricanes and Tropical Meteorology*, Miami Beach, Amer. Meteor. Soc., 43–57.

Golden, J. H. 1976: An assessment of windspeeds in tornadoes. *Proc. Symp. on Tornadoes: Assessment of Knowledge and Implications for Man*, Inst. for Disaster Research, Texas Tech University, Lubbock, 5–42.

Graham, H. E., and G. N. Hudson, 1960: Surface winds near the center of hurricanes (and other cyclones). NHRP Rep. No. 39, U.S. Dept. Commerce, 200 pp. [NOAA/NHRL, 1320 S. Dixie Hwy., Coral Gables, FL 33146].

Hebert, P. J., 1980: The Atlantic hurricane season of 1979. *Mon. Wea. Rev.*, **108**, 973–980.

Hubert, L. E., 1955: Frictional filling of hurricanes. *Bull. Amer. Meteor. Soc.*, **36**, 440–445.

——, 1959: Distribution of surface friction in hurricanes. *J. Meteor.*, **16**, 393–403.

Hughes, L. A., 1952: On the low-level wind structure of tropical storms. *J. Meteor.*, **9**, 422–428.

Johnson, R. E., 1954: Estimation of friction of surface winds in the August, 1949, Florida hurricane. *Mon. Wea. Rev.*, **82**, 73–79.

Jorgensen, D. P., 1981: Meso- and convective-scale characteristics common to several mature hurricanes. *Preprints, 20th Conf. on Radar Meteorology*, Boston, Amer. Meteor. Soc., 726–733.

Krueger, D. W., 1959: A relation between the mass circulation through hurricanes and their intensity. *Bull. Amer. Meteor. Soc.*, **40**, 182–189.

Malkin, W., 1959: Filling and intensity changes in hurricanes over land. NHRP Rep. No. 34, U.S. Dept. Commerce, 18 pp. [NOAA/NHRL, 1320 S. Dixie Hwy., Coral Gables, FL 33146].

Miller, B. I., 1958: The three-dimensional wind structure around a tropical cyclone. NHRP Rep. No. 15, U.S. Dept. Commerce, 41 pp. [NOAA/NHRL, 1320 S. Dixie Hwy., Coral Gables, FL 33146].

——, 1963: On the filling of tropical cyclones over land. NHRP Rep. No. 66, U.S. Dept. Commerce, 82 pp. [NOAA/NHRL, 1320 S. Dixie Hwy., Coral Gables, FL 33146].

——, 1964: A study of the filling of Hurricane Donna (1960) over land. *Mon. Wea. Rev.*, **92**, 389–406.

Moss, M. S., and R. W. Jones, 1978: A numerical simulation of hurricane landfall. NOAA Tech. Memo, ERL NHEML-3, U.S. Dept. Commerce, 15 pp. [NOAA/NHRL, 1320 S. Dixie Hwy., Coral Gables, FL 33146].

Myers, V. A., 1954a: Surface friction in a hurricane. *Mon. Wea. Rev.*, **82**, 307–311.

——, 1954b: Characteristics of United States hurricanes pertinent to level design for Lake Okeechobee, Florida. Hydrometeor. Rep. No. 32, U.S. Dept. Commerce, 106 pp. [NOAA/NHRL, 1320 S. Dixie Hwy., Coral Gables, FL 33146].

——, and W. Malkin, 1961: Some properties of hurricane wind fields as deduced from trajectories. NHRP Rep. No. 49, U.S. Dept. Commerce, 45 pp. [NOAA/NHRL, 1320 S. Dixie Hwy., Coral Gables, FL 33146].

Novlan, D. J., and W. M. Gray, 1974: Hurricane-spawned tornados. *Mon. Wea. Rev.,* **102,** 476–488.

Parrish, J. R., R. W. Burpee, F. D. Marks and R. Grebe, 1982: Rainfall patterns observed by digitized radar during landfall of Hurricane Frederic (1979). *Mon. Wea. Rev.,* **110,** 1933–1944.

Pierson, W. J., S. Peteherych and J. C. Wilkerson, 1980: The winds of the comparison data set for the Seasat Gulf of Alaska Experiment. *IEEE J. Ocean Eng.,* **OE-5,** 169–176.

Powell, M. D., 1980: Evaluations of diagnostic marine boundary layer models applied to hurricanes. *Mon. Wea. Rev.,* **108,** 757–766.

Reinhold, T. A., and K. C. Mehta, 1981: Wind damage in Hurricane Frederic. *Proc. Second Specialty Conf. on Dynamic Response of Structures,* Atlanta, Amer. Soc. Civ. Eng., 532–546.

Smith, C. L., 1975: On the intensification of Hurricane Celia (1970). *Mon. Wea. Rev.,* **103,** 131–148.

Tuleya, R. E., and Y. Kurihara, 1978: A numerical simulation of the landfall of tropical cyclones. *J. Atmos. Sci.,* **35,** 242–257.

Willoughby, H. E., J. A. Clos and M. G. Shoreibah, 1981: Concentric eye walls, secondary wind maxima, and the evolution of the hurricane vortex. *J. Atmos. Sci.,* **39,** 395–411.